FERMILAB-PUB-04/284-E

Measurement of the Ratio of B^+ and B^0 Meson Lifetimes

V.M. Abazov,[33] B. Abbott,[70] M. Abolins,[61] B.S. Acharya,[27] M. Adams,[48] T. Adams,[46] M. Agelou,[17] J.-L. Agram,[18] S.H. Ahn,[29] M. Ahsan,[55] G.D. Alexeev,[33] G. Alkhazov,[37] A. Alton,[60] G. Alverson,[59] G.A. Alves,[2] M. Anastasoaie,[32] S. Anderson,[42] B. Andrieu,[16] Y. Arnoud,[13] A. Askew,[74] B. Åsman,[38] O. Atramentov,[53] C. Autermann,[20] C. Avila,[7] F. Badaud,[12] A. Baden,[57] B. Baldin,[47] P.W. Balm,[31] S. Banerjee,[27] E. Barberis,[59] P. Bargassa,[74] P. Baringer,[54] C. Barnes,[40] J. Barreto,[2] J.F. Bartlett,[47] U. Bassler,[16] D. Bauer,[51] A. Bean,[54] S. Beauceron,[16] M. Begel,[66] A. Bellavance,[63] S.B. Beri,[26] G. Bernardi,[16] R. Bernhard,[47,*] I. Bertram,[39] M. Besançon,[17] R. Beuselinck,[40] V.A. Bezzubov,[36] P.C. Bhat,[47] V. Bhatnagar,[26] M. Binder,[24] K.M. Black,[58] I. Blackler,[40] G. Blazey,[49] F. Blekman,[31] S. Blessing,[46] D. Bloch,[18] U. Blumenschein,[22] A. Boehnlein,[47] O. Boeriu,[52] T.A. Bolton,[55] F. Borcherding,[47] G. Borissov,[39] K. Bos,[31] T. Bose,[65] A. Brandt,[72] R. Brock,[61] G. Brooijmans,[65] A. Bross,[47] N.J. Buchanan,[46] D. Buchholz,[50] M. Buehler,[48] V. Buescher,[22] S. Burdin,[47] T.H. Burnett,[76] E. Busato,[16] J.M. Butler,[58] J. Bystricky,[17] W. Carvalho,[3] B.C.K. Casey,[71] N.M. Cason,[52] H. Castilla-Valdez,[30] S. Chakrabarti,[27] D. Chakraborty,[49] K.M. Chan,[66] A. Chandra,[27] D. Chapin,[71] F. Charles,[18] E. Cheu,[42] L. Chevalier,[17] D.K. Cho,[66] S. Choi,[45] T. Christiansen,[24] L. Christofek,[54] D. Claes,[63] B. Clément,[18] C. Clément,[38] Y. Coadou,[5] M. Cooke,[74] W.E. Cooper,[47] D. Coppage,[54] M. Corcoran,[74] J. Coss,[19] A. Cothenet,[14] M.-C. Cousinou,[14] S. Crépé-Renaudin,[13] M. Cristetiu,[45] M.A.C. Cummings,[49] D. Cutts,[71] H. da Motta,[2] B. Davies,[39] G. Davies,[40] G.A. Davis,[50] K. De,[72] P. de Jong,[31] S.J. de Jong,[32] E. De La Cruz-Burelo,[30] C. De Oliveira Martins,[3] S. Dean,[41] F. Déliot,[17] P.A. Delsart,[19] M. Demarteau,[47] R. Demina,[66] P. Demine,[17] D. Denisov,[47] S.P. Denisov,[36] S. Desai,[67] H.T. Diehl,[47] M. Diesburg,[47] M. Doidge,[39] H. Dong,[67] S. Doulas,[59] L. Duflot,[15] S.R. Dugad,[27] A. Duperrin,[14] J. Dyer,[61] A. Dyshkant,[49] M. Eads,[49] D. Edmunds,[61] T. Edwards,[41] J. Ellison,[45] J. Elmsheuser,[24] J.T. Eltzroth,[72] V.D. Elvira,[47] S. Eno,[57] P. Ermolov,[35] O.V. Eroshin,[36] J. Estrada,[47] D. Evans,[40] H. Evans,[65] A. Evdokimov,[34] V.N. Evdokimov,[36] J. Fast,[47] S.N. Fatakia,[58] L. Feligioni,[58] T. Ferbel,[66] F. Fiedler,[24] F. Filthaut,[32] W. Fisher,[64] H.E. Fisk,[47] M. Fortner,[49] H. Fox,[22] W. Freeman,[47] S. Fu,[47] S. Fuess,[47] T. Gadfort,[76] C.F. Galea,[32] E. Gallas,[47] E. Galyaev,[52] C. Garcia,[66] A. Garcia-Bellido,[76] J. Gardner,[54] V. Gavrilov,[34] P. Gay,[12] D. Gelé,[18] R. Gelhaus,[45] K. Genser,[47] C.E. Gerber,[48] Y. Gershtein,[71] G. Ginther,[66] T. Golling,[21] B. Gómez,[7] K. Gounder,[47] A. Goussiou,[52] P.D. Grannis,[67] S. Greder,[18] H. Greenlee,[47] Z.D. Greenwood,[56] E.M. Gregores,[4] Ph. Gris,[12] J.-F. Grivaz,[15] L. Groer,[65] S. Grünendahl,[47] M.W. Grünewald,[28] S.N. Gurzhiev,[36] G. Gutierrez,[47] P. Gutierrez,[70] A. Haas,[65] N.J. Hadley,[57] S. Hagopian,[46] I. Hall,[70] R.E. Hall,[44] C. Han,[60] L. Han,[41] K. Hanagaki,[47] K. Harder,[55] R. Harrington,[59] J.M. Hauptman,[53] R. Hauser,[61] J. Hays,[50] T. Hebbeker,[20] D. Hedin,[49] J.M. Heinmiller,[48] A.P. Heinson,[45] U. Heintz,[58] C. Hensel,[54] G. Hesketh,[59] M.D. Hildreth,[52] R. Hirosky,[75] J.D. Hobbs,[67] B. Hoeneisen,[11] M. Hohlfeld,[23] S.J. Hong,[29] R. Hooper,[71] P. Houben,[31] Y. Hu,[67] J. Huang,[51] I. Iashvili,[45] R. Illingworth,[47] A.S. Ito,[47] S. Jabeen,[54] M. Jaffré,[15] S. Jain,[70] V. Jain,[68] K. Jakobs,[22] A. Jenkins,[40] R. Jesik,[40] K. Johns,[42] M. Johnson,[47] A. Jonckheere,[47] P. Jonsson,[40] H. Jöstlein,[47] A. Juste,[47] M.M. Kado,[43] D. Käfer,[20] W. Kahl,[55] S. Kahn,[68] E. Kajfasz,[14] A.M. Kalinin,[33] J. Kalk,[61] D. Karmanov,[35] J. Kasper,[58] D. Kau,[46] R. Kehoe,[73] S. Kermiche,[14] S. Kesisoglou,[71] A. Khanov,[66] A. Kharchilava,[52] Y.M. Kharzheev,[33] K.H. Kim,[29] B. Klima,[47] M. Klute,[21] J.M. Kohli,[26] M. Kopal,[70] V.M. Korablev,[36] J. Kotcher,[68] B. Kothari,[65] A. Koubarovsky,[35] A.V. Kozelov,[36] J. Kozminski,[61] S. Krzywdzinski,[47] S. Kuleshov,[34] Y. Kulik,[47] S. Kunori,[57] A. Kupco,[17] T. Kurča,[19] S. Lager,[38] N. Lahrichi,[17] G. Landsberg,[71] J. Lazoflores,[46] A.-C. Le Bihan,[18] P. Lebrun,[19] S.W. Lee,[29] W.M. Lee,[46] A. Leflat,[35] F. Lehner,[47,*] C. Leonidopoulos,[65] P. Lewis,[40] J. Li,[72] Q.Z. Li,[47] J.G.R. Lima,[49] D. Lincoln,[47] S.L. Linn,[46] J. Linnemann,[61] V.V. Lipaev,[36] R. Lipton,[47] L. Lobo,[40] A. Lobodenko,[37] M. Lokajicek,[10] A. Lounis,[18] H.J. Lubatti,[76] L. Lueking,[47] M. Lynker,[52] A.L. Lyon,[47] A.K.A. Maciel,[49] R.J. Madaras,[43] P. Mättig,[25] A. Magerkurth,[60] A.-M. Magnan,[13] N. Makovec,[15] P.K. Mal,[27] S. Malik,[56] V.L. Malyshev,[33] H.S. Mao,[6] Y. Maravin,[47] M. Martens,[47] S.E.K. Mattingly,[71] A.A. Mayorov,[36] R. McCarthy,[67] R. McCroskey,[42] D. Meder,[23] H.L. Melanson,[47] A. Melnitchouk,[62] M. Merkin,[35] K.W. Merritt,[47] A. Meyer,[20] H. Miettinen,[74] D. Mihalcea,[49] J. Mitrevski,[65] N. Mokhov,[47] J. Molina,[3] N.K. Mondal,[27] H.E. Montgomery,[47] R.W. Moore,[5] G.S. Muanza,[19] M. Mulders,[47] Y.D. Mutaf,[67] E. Nagy,[14] M. Narain,[58] N.A. Naumann,[32] H.A. Neal,[60] J.P. Negret,[7] S. Nelson,[46] P. Neustroev,[37] C. Noeding,[22] A. Nomerotski,[47] S.F. Novaes,[4] T. Nunnemann,[24] E. Nurse,[41] V. O'Dell,[47] D.C. O'Neil,[5] V. Oguri,[3] N. Oliveira,[3] N. Oshima,[47] G.J. Otero y Garzón,[48] P. Padley,[74] N. Parashar,[56] J. Park,[29] S.K. Park,[29] J. Parsons,[65] R. Partridge,[71] N. Parua,[67] A. Patwa,[68] P.M. Perea,[45] E. Perez,[17] O. Peters,[31]

P. Pétroff,[15] M. Petteni,[40] L. Phaf,[31] R. Piegaia,[1] P.L.M. Podesta-Lerma,[30] V.M. Podstavkov,[47] Y. Pogorelov,[52] B.G. Pope,[61] W.L. Prado da Silva,[3] H.B. Prosper,[46] S. Protopopescu,[68] M.B. Przybycien,[50,†] J. Qian,[60] A. Quadt,[21] B. Quinn,[62] K.J. Rani,[27] P.A. Rapidis,[47] P.N. Ratoff,[39] N.W. Reay,[55] S. Reucroft,[59] M. Rijssenbeek,[67] I. Ripp-Baudot,[18] F. Rizatdinova,[55] C. Royon,[17] P. Rubinov,[47] R. Ruchti,[52] G. Sajot,[13] A. Sánchez-Hernández,[30] M.P. Sanders,[41] A. Santoro,[3] G. Savage,[47] L. Sawyer,[56] T. Scanlon,[40] R.D. Schamberger,[67] H. Schellman,[50] P. Schieferdecker,[24] C. Schmitt,[25] A.A. Schukin,[36] A. Schwartzman,[64] R. Schwienhorst,[61] S. Sengupta,[46] H. Severini,[70] E. Shabalina,[48] M. Shamim,[55] V. Shary,[17] W.D. Shephard,[52] D. Shpakov,[59] R.A. Sidwell,[55] V. Simak,[9] V. Sirotenko,[47] P. Skubic,[70] P. Slattery,[66] R.P. Smith,[47] K. Smolek,[9] G.R. Snow,[63] J. Snow,[69] S. Snyder,[68] S. Söldner-Rembold,[41] X. Song,[49] Y. Song,[72] L. Sonnenschein,[58] A. Sopczak,[39] M. Sosebee,[72] K. Soustruznik,[8] M. Souza,[2] B. Spurlock,[72] N.R. Stanton,[55] J. Stark,[13] J. Steele,[56] G. Steinbrück,[65] K. Stevenson,[51] V. Stolin,[34] A. Stone,[48] D.A. Stoyanova,[36] J. Strandberg,[38] M.A. Strang,[72] M. Strauss,[70] R. Ströhmer,[24] M. Strovink,[43] L. Stutte,[47] S. Sumowidagdo,[46] A. Sznajder,[3] M. Talby,[14] P. Tamburello,[42] W. Taylor,[5] P. Telford,[41] J. Temple,[42] S. Tentindo-Repond,[46] E. Thomas,[14] B. Thooris,[17] M. Tomoto,[47] T. Toole,[57] J. Torborg,[52] S. Towers,[67] T. Trefzger,[23] S. Trincaz-Duvoid,[16] B. Tuchming,[17] C. Tully,[64] A.S. Turcot,[68] P.M. Tuts,[65] L. Uvarov,[37] S. Uvarov,[37] S. Uzunyan,[49] B. Vachon,[5] R. Van Kooten,[51] W.M. van Leeuwen,[31] N. Varelas,[48] E.W. Varnes,[42] I.A. Vasilyev,[36] M. Vaupel,[25] P. Verdier,[15] L.S. Vertogradov,[33] M. Verzocchi,[57] F. Villeneuve-Seguier,[40] J.-R. Vlimant,[16] E. Von Toerne,[55] M. Vreeswijk,[31] T. Vu Anh,[15] H.D. Wahl,[46] R. Walker,[40] L. Wang,[57] Z.-M. Wang,[67] J. Warchol,[52] M. Warsinsky,[21] G. Watts,[76] M. Wayne,[52] M. Weber,[47] H. Weerts,[61] M. Wegner,[20] N. Wermes,[21] A. White,[72] V. White,[47] D. Whiteson,[43] D. Wicke,[47] D.A. Wijngaarden,[32] G.W. Wilson,[54] S.J. Wimpenny,[45] J. Wittlin,[58] M. Wobisch,[47] J. Womersley,[47] D.R. Wood,[59] T.R. Wyatt,[41] Q. Xu,[60] N. Xuan,[52] R. Yamada,[47] M. Yan,[57] T. Yasuda,[47] Y.A. Yatsunenko,[33] Y. Yen,[25] K. Yip,[68] S.W. Youn,[50] J. Yu,[72] A. Yurkewicz,[61] A. Zabi,[15] A. Zatserklyaniy,[49] M. Zdrazil,[67] C. Zeitnitz,[23] D. Zhang,[47] X. Zhang,[70] T. Zhao,[76] Z. Zhao,[60] B. Zhou,[60] J. Zhu,[57] M. Zielinski,[66] D. Zieminska,[51] A. Zieminski,[51] R. Zitoun,[67] V. Zutshi,[49] E.G. Zverev,[35] and A. Zylberstejn[17]

(DØ Collaboration)

[1] *Universidad de Buenos Aires, Buenos Aires, Argentina*
[2] *LAFEX, Centro Brasileiro de Pesquisas Físicas, Rio de Janeiro, Brazil*
[3] *Universidade do Estado do Rio de Janeiro, Rio de Janeiro, Brazil*
[4] *Instituto de Física Teórica, Universidade Estadual Paulista, São Paulo, Brazil*
[5] *Simon Fraser University, Burnaby, Canada, University of Alberta, Edmonton, Canada, McGill University, Montreal, Canada and York University, Toronto, Canada*
[6] *Institute of High Energy Physics, Beijing, People's Republic of China*
[7] *Universidad de los Andes, Bogotá, Colombia*
[8] *Charles University, Center for Particle Physics, Prague, Czech Republic*
[9] *Czech Technical University, Prague, Czech Republic*
[10] *Institute of Physics, Academy of Sciences, Center for Particle Physics, Prague, Czech Republic*
[11] *Universidad San Francisco de Quito, Quito, Ecuador*
[12] *Laboratoire de Physique Corpusculaire, IN2P3-CNRS, Université Blaise Pascal, Clermont-Ferrand, France*
[13] *Laboratoire de Physique Subatomique et de Cosmologie, IN2P3-CNRS, Universite de Grenoble 1, Grenoble, France*
[14] *CPPM, IN2P3-CNRS, Université de la Méditerranée, Marseille, France*
[15] *Laboratoire de l'Accélérateur Linéaire, IN2P3-CNRS, Orsay, France*
[16] *LPNHE, Universités Paris VI and VII, IN2P3-CNRS, Paris, France*
[17] *DAPNIA/Service de Physique des Particules, CEA, Saclay, France*
[18] *IReS, IN2P3-CNRS, Université Louis Pasteur, Strasbourg, France and Université de Haute Alsace, Mulhouse, France*
[19] *Institut de Physique Nucléaire de Lyon, IN2P3-CNRS, Université Claude Bernard, Villeurbanne, France*
[20] *RWTH Aachen, III. Physikalisches Institut A, Aachen, Germany*
[21] *Universität Bonn, Physikalisches Institut, Bonn, Germany*
[22] *Universität Freiburg, Physikalisches Institut, Freiburg, Germany*
[23] *Universität Mainz, Institut für Physik, Mainz, Germany*
[24] *Ludwig-Maximilians-Universität München, München, Germany*
[25] *Fachbereich Physik, University of Wuppertal, Wuppertal, Germany*
[26] *Panjab University, Chandigarh, India*
[27] *Tata Institute of Fundamental Research, Mumbai, India*
[28] *University College Dublin, Dublin, Ireland*
[29] *Korea Detector Laboratory, Korea University, Seoul, Korea*
[30] *CINVESTAV, Mexico City, Mexico*
[31] *FOM-Institute NIKHEF and University of Amsterdam/NIKHEF, Amsterdam, The Netherlands*
[32] *University of Nijmegen/NIKHEF, Nijmegen, The Netherlands*
[33] *Joint Institute for Nuclear Research, Dubna, Russia*

[34] *Institute for Theoretical and Experimental Physics, Moscow, Russia*
[35] *Moscow State University, Moscow, Russia*
[36] *Institute for High Energy Physics, Protvino, Russia*
[37] *Petersburg Nuclear Physics Institute, St. Petersburg, Russia*
[38] *Lund University, Lund, Sweden, Royal Institute of Technology and Stockholm University, Stockholm, Sweden and Uppsala University, Uppsala, Sweden*
[39] *Lancaster University, Lancaster, United Kingdom*
[40] *Imperial College, London, United Kingdom*
[41] *University of Manchester, Manchester, United Kingdom*
[42] *University of Arizona, Tucson, Arizona 85721, USA*
[43] *Lawrence Berkeley National Laboratory and University of California, Berkeley, California 94720, USA*
[44] *California State University, Fresno, California 93740, USA*
[45] *University of California, Riverside, California 92521, USA*
[46] *Florida State University, Tallahassee, Florida 32306, USA*
[47] *Fermi National Accelerator Laboratory, Batavia, Illinois 60510, USA*
[48] *University of Illinois at Chicago, Chicago, Illinois 60607, USA*
[49] *Northern Illinois University, DeKalb, Illinois 60115, USA*
[50] *Northwestern University, Evanston, Illinois 60208, USA*
[51] *Indiana University, Bloomington, Indiana 47405, USA*
[52] *University of Notre Dame, Notre Dame, Indiana 46556, USA*
[53] *Iowa State University, Ames, Iowa 50011, USA*
[54] *University of Kansas, Lawrence, Kansas 66045, USA*
[55] *Kansas State University, Manhattan, Kansas 66506, USA*
[56] *Louisiana Tech University, Ruston, Louisiana 71272, USA*
[57] *University of Maryland, College Park, Maryland 20742, USA*
[58] *Boston University, Boston, Massachusetts 02215, USA*
[59] *Northeastern University, Boston, Massachusetts 02115, USA*
[60] *University of Michigan, Ann Arbor, Michigan 48109, USA*
[61] *Michigan State University, East Lansing, Michigan 48824, USA*
[62] *University of Mississippi, University, Mississippi 38677, USA*
[63] *University of Nebraska, Lincoln, Nebraska 68588, USA*
[64] *Princeton University, Princeton, New Jersey 08544, USA*
[65] *Columbia University, New York, New York 10027, USA*
[66] *University of Rochester, Rochester, New York 14627, USA*
[67] *State University of New York, Stony Brook, New York 11794, USA*
[68] *Brookhaven National Laboratory, Upton, New York 11973, USA*
[69] *Langston University, Langston, Oklahoma 73050, USA*
[70] *University of Oklahoma, Norman, Oklahoma 73019, USA*
[71] *Brown University, Providence, Rhode Island 02912, USA*
[72] *University of Texas, Arlington, Texas 76019, USA*
[73] *Southern Methodist University, Dallas, Texas 75275, USA*
[74] *Rice University, Houston, Texas 77005, USA*
[75] *University of Virginia, Charlottesville, Virginia 22901, USA*
[76] *University of Washington, Seattle, Washington 98195, USA*

(Dated: October 19, 2004)

The ratio of B^+ and B^0 meson lifetimes was measured using data collected in 2002–2004 by the DØ experiment in Run II of the Fermilab Tevatron Collider. These mesons were reconstructed in $B \to \mu^+\nu D^{*-}X$ decays, which are dominated by B^0, and $B \to \mu^+\nu\bar{D}^0X$ decays, which are dominated by B^+. The ratio of lifetimes is measured to be $\tau^+/\tau^0 = 1.080 \pm 0.016$ (stat)± 0.014 (syst).

PACS numbers: 14.40.Nd

In the last few years, significant progress has been made, on both experimental and theoretical fronts, in the understanding of the lifetimes of hadrons containing heavy quarks. Charm and bottom meson (except B_c) lifetimes have been measured with precisions ranging from 0.5% to 4%, although lifetimes of heavy baryons are not known as well [1]. On the theoretical front, predictions are being made using a rigorous approach based on the heavy quark expansion (in negative powers of the heavy quark mass) [2], where the large mass of the bottom quark considerably simplifies calculations. Theoretical uncertainties are further reduced for ratios of lifetimes. For instance, the ratio of the B^+ and B^0 lifetimes has been predicted to be 1.06 ± 0.02 [3]. Experimentally, ratios of lifetimes have smaller uncertainties, since many common sources of systematics cancel.

In this Letter, we present a measurement of the ratio of B^+ and B^0 lifetimes using a large sample of semileptonic B decays collected by the DØ experiment at Fermilab in $p\bar{p}$ collisions at $\sqrt{s} = 1.96$ TeV. The data correspond to approximately 440 pb^{-1} of integrated luminosity. B mesons were selected via their decays $B \to \mu^+\nu\bar{D}^0X$ [4] and were classified into two exclusive groups: a "D^{*-}" sample, containing all events with reconstructed $D^{*-} \to \bar{D}^0\pi^-$ decays, and a "$\bar{D}^0$" sample, containing all remaining events. Both simulation and available experimental results show that the D^{*-} sample is dominated by $B^0 \to \mu^+\nu D^{*-}X$ decays, while the $\bar{D}^0$ sample is dominated by $B^+ \to \mu^+\nu\bar{D}^0X$ decays.

The classification into these two samples was based on the presence of a slow pion from $D^{*-} \to \bar{D}^0\pi^-$ decay, and thus was independent of the B-meson lifetime. Therefore, the ratio of the number of events in the two samples, expressed as a function of the proper decay length, depends mainly on the lifetime difference between the B^+ and B^0 mesons. The influences of the selection criteria, detector properties, and some systematic uncertainties are significantly reduced.

The DØ detector is described in detail elsewhere [5]. The detector components most important to this analysis are the central tracking and muon systems. The tracking system consists of a silicon microstrip tracker and a central fiber tracker, both located within a 2 T superconducting solenoidal magnet. The resolution for the distance of closest approach as provided by the tracking system is ≈ 50 μm for tracks with $p_T \approx 1$ GeV/c, improving asymptotically to 15 μm for tracks with $p_T \geq 10$ GeV/c, where p_T is the component of the momentum perpendicular to the beam pipe. The muon system is located outside the calorimeters and consists of a layer of drift chambers and scintillation trigger counters in front of 1.8 T toroids, followed by two more similar layers after the toroids.

Events with semi-muonic b-hadron decays were selected using a suite of inclusive single-muon triggers in a three-level trigger system. Muons were identified by extrapolating tracks found in the central tracking system and matching them with muon track segments formed from hits in the muon system. Muons were required to have a transverse momentum $p_T^\mu > 2$ GeV/c and total momentum $p^\mu > 3$ GeV/c.

The primary vertex of the $p\bar{p}$ interaction was determined for each event. The average position of the beam-collision point was included as a constraint. The precision of the primary vertex reconstruction was on average about 20 μm in the plane perpendicular to the beam direction and about 40 μm along the beam direction.

$\bar{D}^0$ candidates were selected using their $\bar{D}^0 \to K^+\pi^-$ decay mode. All charged particles in an event were clustered into jets using the DURHAM clustering algorithm [6] with a jet p_T cut-off parameter of 15 GeV/c [7]. The $\bar{D}^0$ candidate was constructed from two particles of opposite charge belonging to the same jet as the reconstructed muon. Both particles were required to have $p_T > 0.7$ GeV/c and to form a common $\bar{D}^0$ vertex. The p_T of the $\bar{D}^0$ was required to exceed 5 GeV/c. To reduce combinatorial background, we required the $\bar{D}^0$ vertex to have a positive displacement in the xy plane, relative to the primary vertex, with at least 4σ significance. Although this last requirement can bias the lifetime distribution of a B candidate, our analysis procedure of determining the ratio of B^+ and B^0 events in bins of proper time should remove this bias in the final result. The trajectory of the muon and $\bar{D}^0$ candidates were required to originate from a common B vertex. The $\mu^+\bar{D}^0$ system was required to have an invariant mass between 2.3 and 5.2 GeV/c^2.

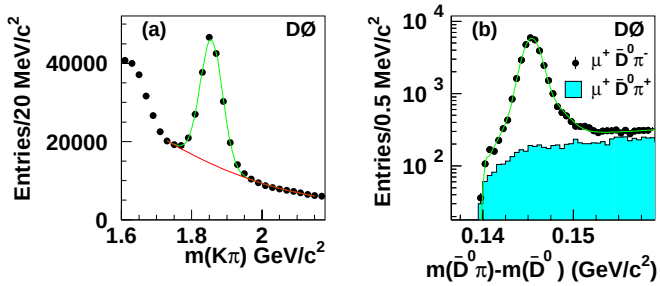

FIG. 1: (a) Invariant mass of the $K\pi$ system. The curve shows the result of the fit of the $K^+\pi^-$ mass distribution with the sum of a signal Gaussian function and polynomial background function. (b) Mass difference $\Delta m = m(\bar{D}^0\pi) - m(\bar{D}^0)$.

The masses of the kaon and pion were assigned to the two tracks according to the charge of the muon, assuming the $\mu^+K^+\pi^-$ combination. The mass spectrum of the $K\pi$ system after these selections is shown in Fig. 1(a). The signal in the $\bar{D}^0$ peak contains 126073 ± 610 events.

All reconstructed $\mu^+\bar{D}^0$ events were classified into three non-overlapping samples. For each $\mu^+\bar{D}^0$ candidate, a search was made for an additional pion. The mass difference $\Delta m = m(\bar{D}^0\pi) - m(\bar{D}^0)$ for all such pions, when $1.8 < m(\bar{D}^0) < 1.9$ GeV/c^2, is shown in Fig. 1(b). The peak in this figure corresponds to the production of the μ^+D^{*-} system. All events containing a pion with a charge opposite to that of the muon (right-charge combination) and $0.1425 < \Delta m < 0.1490$ GeV/c^2 were included in the D^{*-R} sample. All events containing a pion with the same charge as the muon (wrong-charge combination) and $0.1425 < \Delta m < 0.1490$ GeV/c^2 were included in the auxiliary D^{*-W} sample. This sample contains true $\bar{D}^0$ but fake D^{*-} events and gives an estimate of the combinatorial background for selected μ^+D^{*-} candidates. The Δm distribution for such events is shown in Fig. 1(b) as the filled histogram. All remaining events were assigned to the $\bar{D}^0$ sample.

Since the final (semileptonic) state has missing particles, including the neutrino, the proper decay length was not determined. Instead, for

each reconstructed candidate, the measured visible proper decay length x^M was computed as $x^M = m_B c\left(\boldsymbol{L}_T \cdot \boldsymbol{p}_T(\mu^+\bar{D}^0)\right)/|\boldsymbol{p}_T(\mu^+\bar{D}^0)|^2$. $\boldsymbol{L}_T$ is the vector in the axial plane from the primary to the B-meson decay vertex, $\boldsymbol{p}_T(\mu^+\bar{D}^0)$ is the transverse momentum of the $\mu^+\bar{D}^0$ system and m_B is the mass of the B meson, for which the value 5.279 GeV/c^2 was used [1]. The pion from the D^{*-} decay was not used for the computation of the transverse momentum and the decay length.

Candidates in each of the samples were divided into eight groups according to their x^M value. The number of $\mu^+\bar{D}^0$ events N_i^{*R} (from the D^{*-R} sample), N_i^{*W} (from the D^{*-W} sample), and N_i^0 (from the $\bar{D}^0$ sample) in each interval i (where i ranges from one to eight) were determined from the fit of the $K\pi$ mass spectrum between 1.72 and 2.16 GeV/c^2 with the sum of a Gaussian signal function and a polynomial background function. The mean and width of the Gaussian function were fixed to the values obtained from the fit of the overall mass distribution in each sample. The fitting procedure was the same for all samples. Table I gives the numbers obtained for each x^M interval.

The number of μ^+D^{*-} events for each interval i of x^M was defined as $N_i(\mu^+D^{*-}) = N_i^{*R} - C \cdot N_i^{*W}$, where $C \cdot N_i^{*W}$ accounts for the combinatorial background under the D^{*-} peak as shown in Fig. 1(b). The coefficient $C = 1.27 \pm 0.03$ reflects the difference in the combinatorial background between $\mu^+\bar{D}^0\pi^-$ and $\mu^+\bar{D}^0\pi^+$ events. It was determined from the ratio of the numbers of these events in the interval $0.153 < \Delta m < 0.160$ GeV/c^2. The number of $\mu^+\bar{D}^0$ events in each interval i in x^M was defined as $N_i(\mu^+\bar{D}^0) = N_i^0 + N_i^{*W} + C \cdot N_i^{*W}$.

The experimental observable r_i is the ratio of μ^+D^{*-} and $\mu^+\bar{D}^0$ events in interval i of x^M, i.e., $r_i = N_i(\mu^+D^{*-})/N_i(\mu^+\bar{D}^0)$. Values of r_i and statistical uncertainties are given in Table I. The measurement of the lifetime difference between B^+ and B^0 is given by $k \equiv \tau^+/\tau^0 - 1$. It was determined from the minimization of $\chi^2(\varepsilon_\pi, k)$:

$$\chi^2(\varepsilon_\pi, k) = \sum_i \frac{(r_i - r_i^e(\varepsilon_\pi, k))^2}{\sigma^2(r_i)}, \qquad (1)$$

where $r_i^e(\varepsilon_\pi, k)$ is the expected ratio of μ^+D^{*-} and $\mu^+\bar{D}^0$ events, and ε_π is the efficiency to reconstruct the slow pion in the $D^{*-} \to \bar{D}^0\pi^-$ decay. ε_π was assumed to be independent of x^M and, along with k, was a free parameter in the minimization. We present evidence for the validity of this assumption in the discussion of systematic uncertainties. The sum $\sum_i$ was taken over all intervals with positive x^M.

Information used to determine the expected ratio, $r_i^e(\varepsilon_\pi, k)$, included both experimental measurements as well as results from Monte Carlo simulations. For the jth B-meson decay channel, the distribution of the visible proper decay length (x) is given by $P_j(x) = \int dK\, D_j(K) \cdot \theta(x) \cdot \frac{K}{c\tau_j} \exp(-\frac{Kx}{c\tau_j})$. τ_j is the lifetime of the B meson, the K-factor, $K = p_T^{\mu^+\bar{D}^0}/p_T^B$, reflects the difference between the observed and true momentum of the B meson, and $\theta(x)$ is the step function. The function $D_j(K)$ is the normalized distribution of the K-factor for the jth decay channel.

Transformation from the true value of x to the experimentally measured value x^M is given by $f_j(x^M) = \int dx\, R_j(x - x^M) \cdot \varepsilon_j(x) \cdot P_j(x)$, where $R_j(x - x^M)$ is the detector resolution, and $\varepsilon_j(x)$ is the reconstruction efficiency of $\mu^+\bar{D}^0$ for the jth decay. It does not include ε_π for channels with D^{*-}. Finally, the expected value $r_i^e(\varepsilon_\pi, k)$ is given by:

$$r_i^e(\varepsilon_\pi, k) = \frac{\varepsilon_\pi \cdot F_i^*(k)}{F_i^0(k) + (1 - \varepsilon_\pi) \cdot F_i^*(k)}. \qquad (2)$$

Here $F_i^{*,0} = \int_i dx^M \sum_j Br_j \cdot f_j(x^M)$ with the summation $\sum_j$ taken over all decays to D^{*-} ($\bar{D}^0$) for F_i^* (F_i^0).

For the computation of r_i^e, the world average of the B^+ lifetime [1] was used. The B^0 lifetime τ^0 was expressed as $\tau^0 = \tau^+/(1+k)$. The branching fractions $B \to \mu^+\nu\bar{D}$ and $B \to \mu^+\nu\bar{D}^*$ were taken from Ref. [1]. The following branching fractions were derived from experimental measurements [1, 8–10]: $Br(B^+ \to \mu^+\nu\bar{D}^{**0}) = (2.67 \pm 0.37)\%$, $Br(B^+ \to \mu^+\nu\bar{D}^{**0} \to D^{*-}X) = (1.07 \pm 0.25)\%$, and $Br(B_s^0 \to \mu^+\nu D_{s}^{**-}) = (2.3^{+2.4}_{-2.3})\%$. D^{**} states include both narrow and wide D^{**} resonances and non-resonant DX and D^*X production. Regarding the possible decays of D_s^{**-}, there is no experimental data on the $Br(D_s^{**-} \to D^{*-}X)$. Its central value was therefore set to 0.35 and it was varied between 0.0 and 1.0 to estimate the systematic uncertainty from this source. All other branching fractions were derived assuming isospin invariance.

The distributions $D_j(K)$, $R_j(x)$, and $\varepsilon_j(x)$ were taken from the Monte Carlo simulation, and the corresponding systematic uncertainties were taken into account. All processes involving b hadrons were simulated using the EvtGen [11] generator interfaced to pythia [7] and followed by the full modeling of the detector response and event reconstruction. The semileptonic b-hadron decays were generated using the ISGW2 model [12].

Assuming the given branching fractions and reconstruction efficiencies, the decay $B \to \mu^+D^{*-}X$ contains $(89 \pm 3)\%$ B^0, $(10 \pm 3)\%$ B^+, and $(1 \pm 1)\%$ B_s^0, while the decay $B \to \mu^+\bar{D}^0X$ contains $(83 \pm 3)\%$ B^+, $(15 \pm 4)\%$ B^0, and $(2 \pm 1)\%$ B_s^0.

A special study showed that in addition to the main decay $B \to \mu^+\bar{D}^0X$, the decay $B \to \tau^+\bar{D}^0X \to \mu^+\nu\bar{\nu}\bar{D}^0X$ results in a $(5 \pm 2)\%$ contribution and the process $c\bar{c} \to \mu^+\bar{D}^0X$ a $(10 \pm 7)\%$ contribution to the selected $\mu^+\bar{D}^0$ sample. These processes were taken into account in the analysis.

Using all these inputs, the minimization of the χ^2 distribution, Eq. (1), gives: $k \equiv \tau^+/\tau^0 - 1 = 0.080 \pm$

TABLE I: Definition of the intervals in visible proper decay length, x^M. For each interval i, the number of events in the D^{*-R}, D^{*-W} and $\bar{D}^0$ samples, the ratio r_i, and the expected value r_i^e for $\tau^+/\tau^0 - 1 = 0.080$ are given.

i	x^M range (cm)	N_i^{*R}	N_i^{*W}	N_i^0	r_i	r_i^e
1	$-0.1 - 0.0$	1714 ± 53	89 ± 22	5225 ± 151	0.295 ± 0.015	0.309
2	$0.0 - 0.02$	6213 ± 94	200 ± 28	18134 ± 222	0.321 ± 0.007	0.315
3	$0.02 - 0.04$	5941 ± 91	169 ± 22	17703 ± 208	0.317 ± 0.007	0.313
4	$0.04 - 0.07$	6424 ± 94	213 ± 23	19707 ± 216	0.305 ± 0.006	0.308
5	$0.07 - 0.10$	4029 ± 74	115 ± 17	12885 ± 171	0.295 ± 0.007	0.300
6	$0.10 - 0.15$	3459 ± 68	106 ± 16	11532 ± 162	0.282 ± 0.007	0.291
7	$0.15 - 0.25$	2253 ± 57	58 ± 13	7567 ± 137	0.283 ± 0.009	0.276
8	$0.25 - 0.40$	518 ± 28	2 ± 6	1875 ± 75	0.274 ± 0.019	0.256

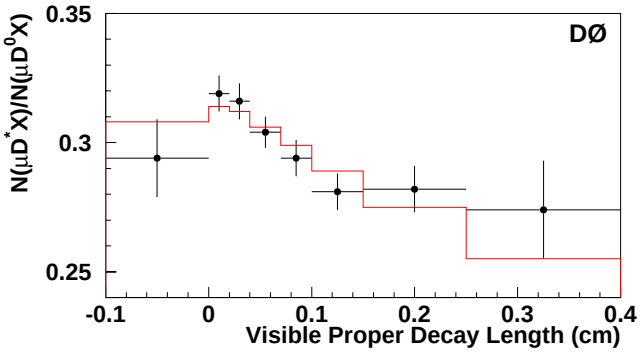

FIG. 2: Points with the error bars show the ratio of the number of events in the μ^+D^{*-} and $\mu^+\bar{D}^0$ samples as a function of the visible proper decay length. The result of the minimization of Eq. (1) with $k = 0.080$ is shown as a histogram.

0.016 (stat). The χ^2 at the minimum is 4.2 for 5 d.o.f, ε_π is 0.864 ± 0.006 (stat), and the global correlation coefficient between k and ε_π is 0.18. The simulation predicted $\varepsilon_\pi = 0.877 \pm 0.003$. The reasonable agreement in ε_π between data and simulation reflects good consistency of input efficiencies and branching fractions with experimental data. Figure 2 presents the r_i values together with the result of the fit.

The influence of various sources of systematic uncertainty on the final result is summarized in Table II. Different contributions can be divided into three groups. The first part includes uncertainties coming from the experimental measurements, e.g., branching fractions and lifetimes. All inputs were varied by one standard deviation. Only the most significant contributions are listed as individual entries in Table II; all remaining uncertainties are combined into a single entry "other contributions."

The second group includes uncertainties due to the inputs taken from the Monte Carlo simulation. They were estimated as follows. The uncertainty due to the decay length dependence of the efficiencies $\varepsilon(B \to \mu^+\nu\bar{D}^0X)$ was obtained by repeating the analysis with decay length independent efficiencies used for all decay modes. This dependence almost cancels in the ratio of the number of events in the two samples, leading to the reduced systematic uncertainty in τ^+/τ^0.

The variation of the efficiency from channel to channel arises from differences in the kinematics of B-meson decays and thus depends on their modeling in simulation. To estimate the uncertainty in the efficiency due to this effect, an alternative HQET model of B-meson decays [13] was implemented, and the selection cuts on the p_T of the μ^+ and $\bar{D}^0$ were varied over a wide range.

The same alternative model and the variation of p_T cuts were used to study the model dependence of the K-factors. In all cases, the variation of the average value of K-factors did not exceed 2%. Distributions of K-factors were determined separately for $B \to \mu^+\nu\bar{D}^0$, $B \to \mu^+\nu\bar{D}^*$, $B \to \mu^+\nu\bar{D}^{**} \to \bar{D}^0X$, and $B \to \mu^+\nu\bar{D}^{**} \to \bar{D}^*X$. To estimate the uncertainty due to the modeling of $\bar{D}^{**}$ decays, which include both resonant and non-resonant components and are not yet well understood, the analysis was repeated with the distributions of K-factors from $B \to \bar{D}^{**} \to \bar{D}^0(\bar{D}^*)$ decays set to be the same as for $B \to \bar{D}^0(\bar{D}^*)$ decays.

The selection of the slow pion was made independently of the B lifetime, and the efficiency ε_π was assumed constant in the minimization. A dedicated study of $K_S \to \pi^+\pi^-$ decays showed good stability of the track reconstruction efficiency with the change of decay length over a wide range. The slope in the efficiency was estimated to be 0.0038 ± 0.0059 cm^{-1}. The independence of ε_π on the decay length was also verified in simulation, where no deviation from the constant value was detected within available simulation statistics.

The average decay length resolution, approximately 35 μm for this measurement, and the fraction of events with larger resolution, modeled by a Gaussian function with resolution of 1700 μm, were varied over a wide range, significantly exceeding the estimated difference in resolution between data and simulation.

The ratio of events with negative decay length in D^{*-} and $\bar{D}^0$ samples (the first row in Table I) is sensitive to the differences in resolution of these two samples. The comparison of this ratio in data with the simulation was used to estimate the systematic uncertainty due to this

TABLE II: Summary of systematic uncertainties.

Source	$\Delta(\tau^+/\tau^0)$
$Br(B^0 \to \mu^+\nu D^{*-})$	0.0005
$Br(B^+ \to \mu^+\nu \bar{D}^{*0})$	0.0010
$Br(B^+ \to \mu^+\nu \bar{D}^{**0})$	0.0009
$Br(B^+ \to \mu^+\nu D^{*-}\pi^+X)$	0.0059
$Br(B_s^0 \to \mu^+\nu D_s^- X)$	0.0009
$D_s^{**-} \to D^{*-}X$	0.0020
$c\bar{c} \to \mu^+\nu\bar{D}^0X$ contribution	0.0015
Other contributions	0.0006
$\varepsilon(B \to \mu^+\nu\bar{D}^0X)$, decay length dependence	0.0014
$\varepsilon(B \to \mu^+\nu\bar{D}^0X)$, average value	0.0030
ε_π, decay length dependence	0.0036
decay length resolution	0.0024
Difference in D^{*-} and $\bar{D}^0$ resolution	0.0053
K-factors, average value	0.0032
K-factors, difference between channels	0.0013
Fitting procedure	0.0086
Background level under D^{*-}	0.0004
Total	**0.0136**

difference.

Since the μ^+D^{*-} and $\mu^+\bar{D}^0$ event yields as a function of proper decay length are extracted by fitting the respective mass distributions with signal and background functional forms, the fitting procedure can be another source of systematic uncertainty. Different parameterizations of signal and background functions were used. The maximal variation of the result obtained was taken as the systematic uncertainty due to this source. Finally, the uncertainty in the background level under the D^{*-} peak in Fig. 1(b) was also taken into account.

Estimated systematic uncertainties from different sources were added in quadrature and the total systematic uncertainty on the ratio of lifetimes is $\sigma(\tau^+/\tau^0) = 0.014$. Various consistency checks of this measurement were also performed. The total sample of events was divided into two parts using different criteria, such as the sign of the muon rapidity, polarity of the solenoid, charge of the muon, p_T of the muon, position of the primary interaction, etc. The measurement was repeated independently for each sample. The definition of proper decay length intervals was varied, one more interval, 0.4 – 0.8 cm, was added, and the last interval, 0.25 – 0.4 cm, was removed from the fit. In all cases, the results are consistent within statistical uncertainties. Finally, the measurement of the ratio of lifetimes was performed with simulated events. The resulting value $k^{\rm MC} = 0.084 \pm 0.015$ agrees well with the generated lifetime ratio $k^{\rm gen} = 0.070$.

In summary, the ratio of B^+ and B^0 meson lifetimes was found to be:

$$k = \frac{\tau^+}{\tau^0} - 1 = 0.080 \pm 0.016\ (\text{stat}) \pm 0.014\ (\text{syst}). \quad (3)$$

This result is the most precise measurement of this parameter, and agrees well with the world average value $k = 0.086 \pm 0.017$ [1]. Improved precision of the ratio of B^+ and B^0 lifetimes will allow a better test of theoretical predictions, especially those inputs to the calculations that rely on lattice QCD or on other non-perturbative methods [2, 3].

We thank the staffs at Fermilab and collaborating institutions, and acknowledge support from the Department of Energy and National Science Foundation (USA), Commissariat à l'Energie Atomique and CNRS/Institut National de Physique Nucléaire et de Physique des Particules (France), Ministry of Education and Science, Agency for Atomic Energy and RF President Grants Program (Russia), CAPES, CNPq, FAPERJ, FAPESP and FUNDUNESP (Brazil), Departments of Atomic Energy and Science and Technology (India), Colciencias (Colombia), CONACyT (Mexico), KRF (Korea), CONICET and UBACyT (Argentina), The Foundation for Fundamental Research on Matter (The Netherlands), PPARC (United Kingdom), Ministry of Education (Czech Republic), Natural Sciences and Engineering Research Council and WestGrid Project (Canada), BMBF and DFG (Germany), A.P. Sloan Foundation, Research Corporation, Texas Advanced Research Program, and the Alexander von Humboldt Foundation.

[*] Visitor from University of Zurich, Zurich, Switzerland.
[†] Visitor from Institute of Nuclear Physics, Krakow, Poland.

[1] S. Eidelman *et al.*, Phys. Lett. B **592**, 1 (2004).
[2] G. Bellini, I. Bigi and P. Dornan, Phys. Rep. **289**, 1 (1997).
[3] C. Tarantino, Eur. Phys. J. **C 33**, s01, s895 (2004), arXiv:hep-ph/0310241.
[4] Charge conjugate states are always implied in this Letter.
[5] V. Abazov *et al.*, in preparation for submission to Nucl. Instrum. Methods Phys. Res. A; T. LeCompte and H.T. Diehl, Ann. Rev. Nucl. Part. Sci. **50**, 71 (2000).
[6] S. Catani *et al.*, Phys. Lett. B **269**, 432 (1991).
[7] T. Sjöstrand *et al.*, Comp. Phys. Commun. **135**, 238 (2001).
[8] D. Buskulic *et al.*, ALEPH Collaboration, Zeit. Phys. **C73**, 601 (1997).
[9] P. Abreu *et al.*, DELPHI Collaboration, Phys. Lett. B **475**, 407 (2000).
[10] D. Abbaneo *et al.*, arXiv:hep-ex/0112028.
[11] D.J. Lange, Nucl. Instrum. Methods Phys. Res. A **462**, 152 (2001).
[12] D. Scora and N. Isgur, Phys. Rev. D **52**, 2783 (1995).
[13] I. Caprini *et al.*, Nucl. Phys. B **530**, 153 (1998).

ADDITIONAL PLOTS

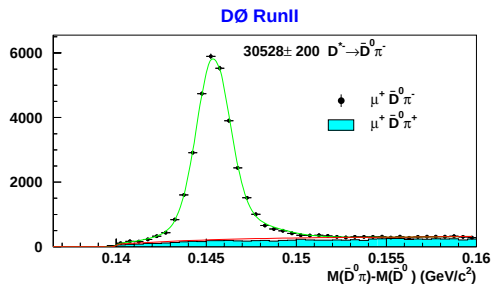

FIG. 3: D^* mass distribution.

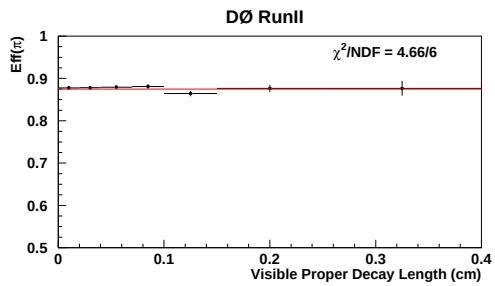

FIG. 4: Efficiencies for slow pions.

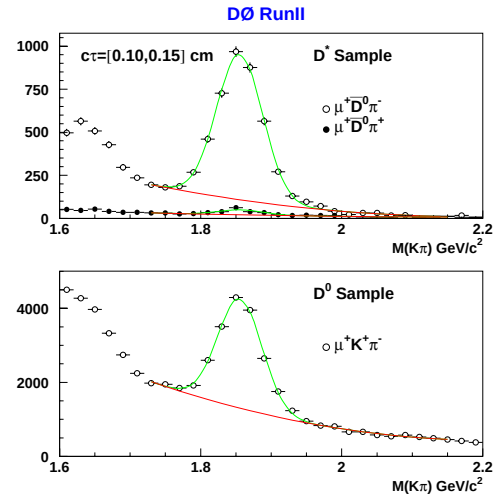

FIG. 5: An example of the fit of the D^0 and D^* ratio in one bin.